ORNL/TM-2024/3309
Rev. 0

Status Report on HFIR Irradiation of Optimized Alumina Forming Alloys

Nuclear Technology Research and Development

Prepared for
US Department of Energy
Nuclear Technology R&D
Advanced Fuels Campaign

Authors:
Annabelle G. Le Coq, David A. Collins, Nick G. Russell, Richard H. Howard, Holden C. Hyer, Sebastien N. Dryepondt, Cody C. Taylor, David T. Hoelzer, Caleb P. Massey
Oak Ridge National Laboratory

March 2024
M3FT-24OR020202053

ACKNOWLEDGMENTS

This research was sponsored by the Advanced Fuels Campaign Program of the US Department of Energy (DOE) Office of Nuclear Energy. Neutron irradiation in the High Flux Isotope Reactor is made possible by the Office of Basic Energy Sciences, US DOE. The report was authored by UT-Battelle LLC under Contract No. DE-AC05-00OR22725 with DOE.

SUMMARY

Properties of FeCrAl alloys under neutron irradiation are of interest because of these materials' potential application as accident-tolerant fuel cladding in nuclear systems. In parallel, alumina-forming austenitic (AFA) alloys are of interest for use as structural materials in advanced nuclear systems for their potential higher resistance to embrittlement and high-temperature steam oxidation resistance. An irradiation campaign for fiscal year 2024 has been developed under the Advanced Fuels Campaign to perform irradiation testing of various FeCrAl and AFA alloys in Oak Ridge National Laboratory's High Flux Isotope Reactor (HFIR). The goals of this irradiation campaign are to (1) study the impact of minor alloying elements on the neutron-irradiated mechanical properties of FeCrAl alloys and (2) collect neutron-irradiated mechanical properties on AFA alloys for comparison with those of FeCrAl alloys. This campaign will include both tensile and fracture toughness specimens tested following HFIR irradiation at temperatures representative of normal operating conditions in light-water reactors. The pre-irradiation characterization to date, the irradiation plan for the FeCrAl and AFA specimens, and the subsequent post-irradiation experimental test plan are presented in this report, along with the status of HFIR builds and scheduled insertion dates.

CONTENTS

FIGURES

TABLES

ACRONYMS

Acronym	Description
AFA	alumina-forming austenitic
AFC	Advanced Fuels Campaign
ATF	Accident-tolerant fuel
BD	build direction
dpa	displacements per atom
EBSD	electron backscatter diffraction
EDS	energy-dispersive x-ray spectroscopy
FY	fiscal year
GE	General Electric
GENTEN	general tensile
HFIR	High Flux Isotope Reactor
HIP	hot-isostatic pressing
ID	inside diameter
IPF	inverse pole figure
LOCA	loss of coolant accident
LPBF	laser powder bed fusion
MBS-1	miniature bend bar slotted 1
MINBEN	miniature bend bar
OD	outside diameter
ORNL	Oak Ridge National Laboratory
PIE	postirradiation examination
RT	room temperature
SEM	scanning electron microscopy
SiC	silicon carbide
TD	transverse direction
TM	thermometry
TRRH	target rod rabbit holder

HFIR CAPSULE READINESS TO SUPPORT TARGETED IRRADIATION OF OPTIMIZED ALUMINA FORMING ALLOYS

1. INTRODUCTION

FeCrAl alloys have been a candidate for accident-tolerant fuel (ATF) cladding since a technology implementation plan was developed for this class of alloys in 2014 by Oak Ridge National Laboratory (ORNL) [1]. Over the past 10 years, significant tensile and fracture toughness data as a function of temperature and dose have been generated on model FeCrAl alloys with respect to various chromium and aluminum alloy compositions, as well as varied grain structures [2][8]. The FeCrAl alloys consistently show significant irradiation hardening and embrittlement at irradiation temperatures below 300°C, associated with high densities of irradiation-induced defects (dislocation loops/black dots) and irradiation-enhanced precipitation (chromium-rich alpha prime phase precipitation).

Initial irradiations of the FeCrAl class of alloys coupled with the rapid iteration of compositions/microstructures have highlighted gaps in our understanding related to how minor alloying elements (molybdenum – solid solution strengthening; yttrium – reactive element effect) impact irradiation induced hardening/embrittlement. Thus, it is of interest to irradiate materials with and without both molybdenum and yttrium to evaluate the effect of these elements on the irradiation hardening/embrittlement of the FeCrAl class of alloys.

A new class of alumina-forming austenitic (AFA) alloys may provide a higher resistance to embrittlement without sacrificing high-temperature steam oxidation resistance for the iron-based alloy. These AFAs were initially developed for fossil applications [9] but are increasingly popular in commercial nuclear power as potential alloys for lead-cooled fast reactor structural materials [10]. Due to their high chromium content and aluminum content, they may provide competitive corrosion and oxidation performance in the presence of high-temperature water/steam as well.

Although AFAs provide an opportunity to pivot away from the embrittlement-prone FeCrAl alloy class, it still remains unclear whether these alloys will provide enough beneficial properties to outweigh potential negatives vs. their ferritic counterpart. For example, AFAs have a lower melting point than that of FeCrAl alloys (1250–1300°C vs. ~1400°C, respectively), but they have 2 to 3 times the strength at loss-of-coolant accident (LOCA)–relevant temperatures—thereby possibly preserving mechanical integrity, minimizing burst openings, and providing additional enhanced accident margin if temperatures remain within the current light water reactor design space. There also remain open questions as to whether AFA neutronic properties can be optimized to minimize further reductions in wall thickness that are necessary to make them economical as fuel cladding in thermalized reactors.

As part of this screening initiative for FeCrAl and AFA alloys, select alloys from both classes of materials will be irradiated in ORNL's High Flux Isotope Reactor (HFIR) as part of a fiscal year (FY) 2024 irradiation campaign. This campaign will include both tensile and fracture toughness specimens tested following irradiation at temperatures representative of normal operating conditions in light-water reactors. The pre-irradiation characterization to date, the irradiation plan for the FeCrAl and AFA specimens, and the subsequent post-irradiation experimental test plan are presented, along with the status of HFIR builds and scheduled insertion dates. The HFIR irradiation capsules are expected to complete irradiation between July and November 2024. Pending available funding in FY25, mechanical tests of lower dose specimens can be harvested for comparison with prior HFIR irradiation data sets.

2. EXPERIMENT CAPSULE DESIGNS

2.1 HFIR

Experiment capsules have been designed at ORNL to support material irradiations in HFIR's flux trap, located at the center of the core (see Figure 1 [11]). Capsules are loaded into a target rod rabbit holder (TRRH), inserted into one of the thirty flux trap target positions. Each TRRH contains 7 axial rabbit positions, noted as TRRH-*a*, *a* being the axial position. Experiments inserted in the flux trap leverage HFIR's highest neutron flux (about 1×10^{15} fast and 2×10^{15} thermal n/cm^2/s) for accelerated accumulation of irradiation damage [11]. HFIR operates at a constant power of 85 MW, for about 6 cycles a year and 25 days per cycle.

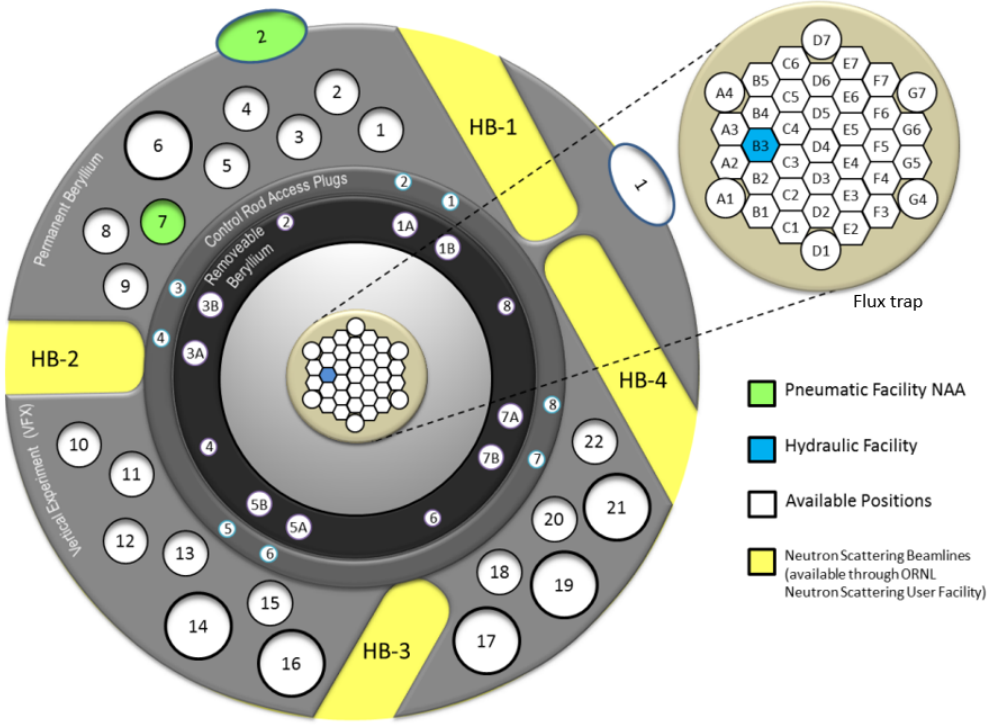

Figure 1. HFIR experiment positions [11].

2.2 Capsule designs

The GENeral TENsile (GENTEN) and the MINiature BENd bar (MINBEN) capsule designs accommodate tensile specimens and bend bar specimens, respectively, for irradiation in HFIR's flux trap [12][13]:

- The GENTEN capsule design comprises three holders, each containing four stacks of 3 SS-J2 specimens (16.0 x 4.0 x 0.5 mm thick), four pieces of passive silicon carbide (SiC) thermometry (TM) that will be analyzed via dilatometry post-irradiation to confirm the irradiation temperature [14], and a roll pin to maintain the stacks of tensile specimens and TMs pressed onto the inner walls of the holder. Thus, a GENTEN capsule accommodates a total of 36 SS-J2 specimens. Figure 2 illustrates the GENTEN capsule design, and more information on this design is available in Champlin et al. [12].

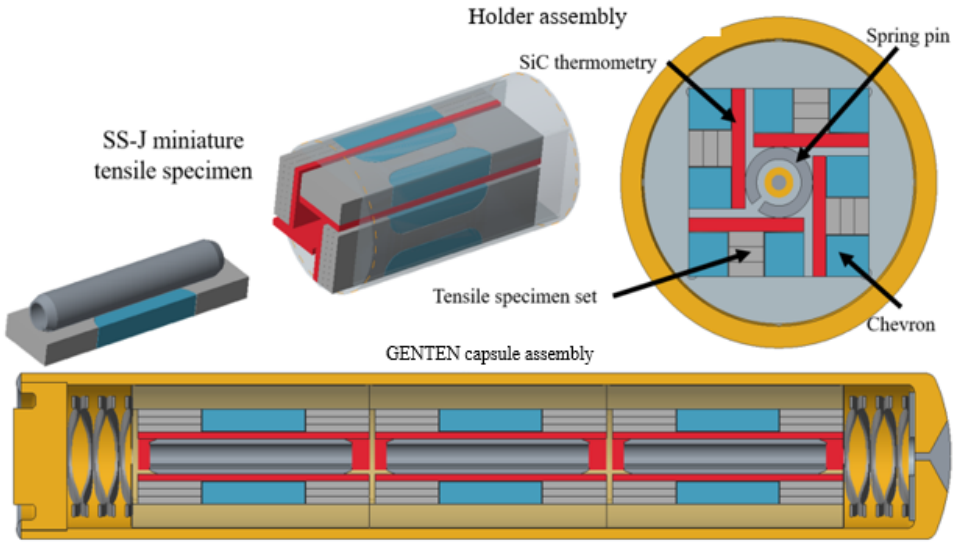

Figure 2. GENTEN capsule design [12].

- The MINBEN capsule design accommodates a total of six miniature bend bar slotted (MBS-1) specimens (14.8 × 4.5 × 3 mm), inserted inside a single holder. Four SiC TMs total are placed in the holder to confirm the irradiation temperature post-irradiation. SiC springs ensure that the MBS-1 specimens are pressed against the walls of the holder and the TMs are pressed against the specimens. An illustration of this design is shown in Figure 3, and more information is available in Champlin et al. [13].

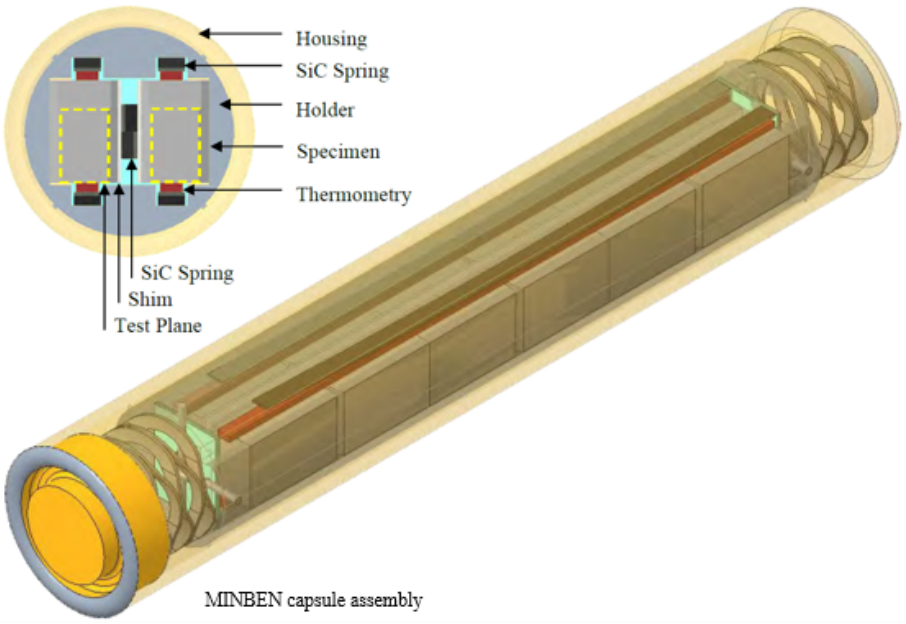

Figure 3. MINBEN capsule design [13].

The design temperature for the GENTEN and MINBEN capsules corresponds to the tensile specimen's average gauge temperature and the bend bar specimen's test plane average temperature, respectively, across the entire duration of the irradiation. The temperature is controlled by varying the fill gas of the capsule (mixture of helium/argon) as well as the gas gap between the outside wall of the holder and the inner wall of the housing. The housing is the external containment of the capsule and is cooled externally by the reactor coolant (at about 60°C). The response surface methodology was employed for both designs to provide target temperatures ranging from 250 to 1100°C (GENTEN) or 650°C (MINBEN) as a function of holder diameter, holder material, gas fill, and TRRH vertical position.

2.3 Thermal results

The GENTEN design provides a relatively uniform average tensile specimen temperature across the capsule: the average TM temperature was about 15°C higher than that of the tensile specimens. An average specimen gauge section temperature of 315°C was obtained in the selected test case using an aluminum holder with an outside diameter (OD) of 9.23 mm, 100% helium fill gas, and a TRRH-3/5 irradiation position. The gauge section presents a temperature distribution of 6–8°C per specimen and a temperature distribution of about 40°C across all the specimens of the capsules. Figure 4 shows the SS-J2 specimen temperature distribution and Table 1 summarizes the temperatures of the TM and specimen gauge section for this test case.

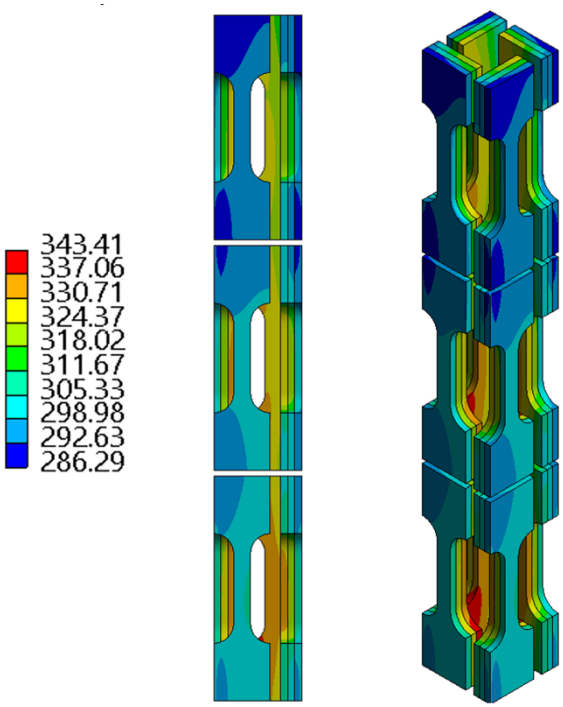

Figure 4. Specimen temperature distribution (in °C) for the GENTEN capsule design using an aluminum holder with an OD of 9.23 mm, 100% helium fill gas, and a TRRH-3/5 irradiation position.

Table 1. Temperatures of the TM and specimen gauge sections for the GENTEN capsule design using an aluminum holder with an OD of 9.23 mm, 100% helium fill gas, and a TRRH-3/5 irradiation position.

Stack location in the capsule		**Top**	**Middle**	**Bottom**	**All**
Component	Temperature (°C)				
TM	Average	330.3	326.6	321.8	326.2
	Min	289.3	286.8	283.5	283.5
	Max	363.1	358.9	353.2	363.1
Inner-most specimen	Average	331.0	327.2	322.3	326.8
	Min	327.4	323.4	318.6	318.6
	Max	333.7	330.0	324.9	333.7
Central specimen	Average	321.6	318.0	313.3	317.5
	Min	318.1	314.3	309.8	309.8
	Max	324.1	320.5	315.7	324.1
Outer-most specimen	Average	304.7	301.4	297.2	301.0
	Min	300.8	297.5	293.5	239.5
	Max	308.5	305.2	300.8	308.5
All specimens	Average	319.1	315.6	310.9	315.1
	Min	300.8	297.5	293.5	293.5
	Max	333.7	330.0	324.9	333.7

The MINBEN thermal analysis described in Champlin et al. [13] considers stainless-steel MBS-1 specimens. For this work, the existing thermal model [13] was updated to consider FeCrAl specimens. The MINBEN FeCrAl test case using an aluminum holder with a 9.26 mm OD, a housing with a 9.519 mm inside diameter (ID), 100% helium fill gas, and a TRRH-3/5 irradiation position was considered. Figure 5 shows the MBS-1 temperature distribution for this test case. This design case resulted in an average specimen test plane temperature of 317°C, with a temperature variation in the test plane across all specimens of the capsule between 281 and 334°C. Table 2 summarizes the specimen test plane and TM temperatures across the capsule for this test case. The specimen test plane temperatures are reported for each pair of specimens located at the top, middle, and bottom of the capsules (test planes 1, 2, and 3, respectively).

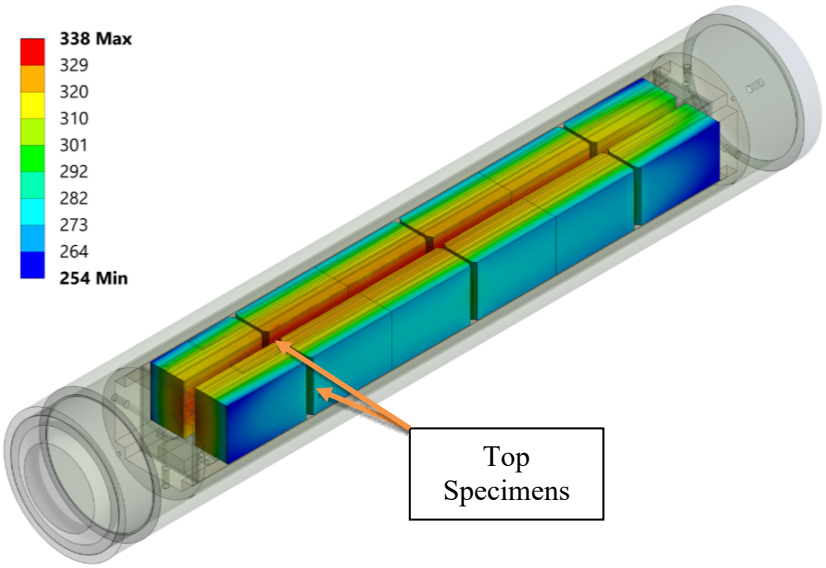

Figure 5. FeCrAl specimen temperature distribution (in °C) for the MINBEN capsule design using an aluminum holder with an OD of 9.26 mm, a housing with a 9.519 mm ID, 100% helium fill gas, and a TRRH-3/5 irradiation position.

Table 2. Temperatures of the FeCrAl specimen test planes and the TM for the MINBEN capsule design for the two test cases.

Test case	Al holder 9.26 mm OD, housing 9.519 mm ID, 100% He, TRRH-3			Al holder 9.27 mm OD, housing 9.504 mm ID, 100% He, TRRH-4		
Component	Temperature (°C)					
	Average	Min.	Max.	Average	Min.	Max.
TM	306	277	316	304	278	313
All specimen test planes	317	281	334	316	277	333
Specimen test planes 1 (top)	318	283	333	313	277	329
Specimen test planes 2 (middle)	320	297	334	319	295	333
Specimen test planes 3 (bottom)	312	281	327	315	281	331

3. IRRADIATION TEST PLAN

3.1 Specimen pre-characterization

A total of 11 AFA/conventional FeCrAl alloys are included in this irradiation test plan. Various alloys were fabricated at ORNL and include wrought material, laser powder bed fusion (LPBF) processed material, and an alloy produced via hot-isostatic press (HIP). Table 3 summarizes the different alloys, giving their compositions and the corresponding type of specimens harvested.

Table 3. AFA and conventional FeCrAl alloys included in the test plan.

Alloy family	Alloy	Comment	Composition	SS-J2 specimen	MBS-1 specimen
AFA	AFA05	LPBF (also referred to as VA05)	Fe-23Ni-17.5Cr-4Al-2Mn-1Mo-0.5W-0.5Si-0.7Nb-0.1Zr-0.1Y-0.5C-0.01B	✓	
	AA06	Heat #21831	Fe-25Ni-16Cr-4Al-2Mo-0.6Nb-0.2Si-0.2Mn-0.03C-0.03Y	✓	✓
	AA07	Heat #21832	Fe-25Ni-16Cr-4Al-2Mo-1.0Nb-0.2Si-0.2Mn-0.03C-0.03Y	✓	✓
	AA09	Heat #21834	Fe-25Ni-16Cr-4Al-2Mo-2.5Nb-0.2Si-0.2Mn-0.03C-0.03Y	✓	✓
Conventional FeCrAl	B126N	Mo-free Variant	Fe-12Cr-6Al+0.2Si	✓	
	C26M0Y	Cr-Variant #1	Fe-12Cr-6Al-2Mo+0.2Si	✓	✓
	C56M0Y	Cr-Variant #2	Fe-15Cr-6Al-2Mo+0.2Si	✓	
	C76M0Y	Cr-Variant #3	Fe-17Cr-6Al-2Mo+0.2Si	✓	
	C26M4	Conventional	Fe-12Cr-6Al-2Mo+0.2Si+0.03Y	✓	✓
	C26M-HIP	Heat #PAC2603	Fe-12Cr-6Al-2Mo+0.2Si	✓	
	C26M-W	Wrought (GE variant)	Fe-12Cr-6Al-2Mo+0.2Si+0.02Y		✓

For the conventional FeCrAl alloys, it was of interest to evaluate alloys with a constant aluminum content but with varied chromium content to establish the effect of chromium content on post-irradiation ductility loss fracture toughness degradation due to the Fe–Cr phase separation phenomenon. Previous irradiations included only materials with simultaneously varying chromium/aluminum content [15] and/or systematically changing aluminum content [16]. As such, for the wrought FeCrAl materials, alloys with varied chromium contents in the 12–17 wt% range were produced. These alloys (C26M0Y, C56M0Y, C76M0Y) also have a "0Y" designation, indicating that there was no yttrium addition to these alloys to remove any effects of intermetallic formation on subsequent ductility loss.

The other three effects probed in this irradiation on FeCrAl alloys include (1) the effect of minor alloying elements, (2) the effect of processing methodology, and (3) the effect of grain size. To assess yttrium addition, conventional C26M4 was included to compare with yttrium-free C26M0Y. To assess molybdenum addition, the molybdenum-free B126N alloy was included. To assess grain size effects, an additional fine-grained variant provided by General Electric (GE) was also included for comparison to

C26M4. Finally, a HIP variant of C26M (without Y) was also included in the experimental test matrix since the HIP process can produce a more refined, uniform, and equiaxed microstructure to compare with the wrought alloys.

AFAs can be considered as a family of alloys rather than a specific alloy. As such, specific compositions of AFA can be tuned to provide a balance between neutronic properties, mechanical properties, and environmental degradation resistance. In the realm of ATF cladding materials, high-temperature resistance to deformation is desired, but the existence of many secondary strengthening phases may adversely affect low-temperature irradiation performance. Four alloys of interest were chosen for the current screening investigation. First, a recently produced AFA, AFA05 (also referred to as VA05) was produced via LPBF and has been shown to provide superior high-temperature creep strength versus conventionally manufactured variants. In addition, three wrought AFAs, with varying niobium content, have been produced to provide different volume fractions of secondary MX carbide phases.

3.1.1 Scanning electron microscopy (SEM)

Each material was pre-characterized using scanning electron microscopy SEM. More specifically, electron backscatter diffraction (EBSD) was conducted on each specimen to obtain an understanding of the grain size, grain morphology, and preferred grain orientation for each alloy. A TESCAN MIRA3 scanning electron microscope with an Oxford Instruments Symmetry EBSD detector, also equipped with energy-dispersive x-ray spectroscopy (EDS) capabilities was used for the pre-irradiation characterization results in this work. For EBSD analysis, the step size was chosen to resolve the grain structures as a function of grain size for each alloy. For the wrought FeCrAl alloys with relatively large grain sizes, the scans covered 2000×1500 μm with a step size of 2 μm. For C26M-HIP, the scan covered 250×200 μm with a step size of 0.5 μm. For the AFA materials, scans were collected across 800×800 μm with a step size of 2 μm.

The general trends in wrought FeCrAl alloy microstructure following identical hot forging, hot rolling, and annealing treatments are provided in Figure 6. Although the same thickness reductions and annealing treatments were performed on each alloy, the differences in minor alloying elements (such as molybdenum and yttrium) were observed to have a significant effect on the final grain structure. Alloys without yttrium deviated from expected equiaxed grain morphologies; instead, these alloys experienced grain elongation along the rolling direction. Conversely, the yttrium-containing alloys had equiaxed grain morphologies and appear to be in the fully recrystallized condition. All of the ORNL-produced, conventional wrought FeCrAl alloys in this work have grain sizes above 100 μm. It is important to note that the EBSD images show alloys such as C36M and C36M-0Y that are not directly included in the irradiation matrix. Since the Cr contents of 12% and 13% were very similar, it was decided to omit including the C36M alloys due to the extensive prior irradiation data on these wrought alloys in the previous FeCrAl irradiation campaigns. In addition, alloys C56M and C76M were not included in the irradiation campaign since the effect of Mo was already included in the C26M comparisons and the effect of Cr could already be investigated in a more straightforward manner without the confounding effects of additional Y-containing intermetallic phases in the microstructure.

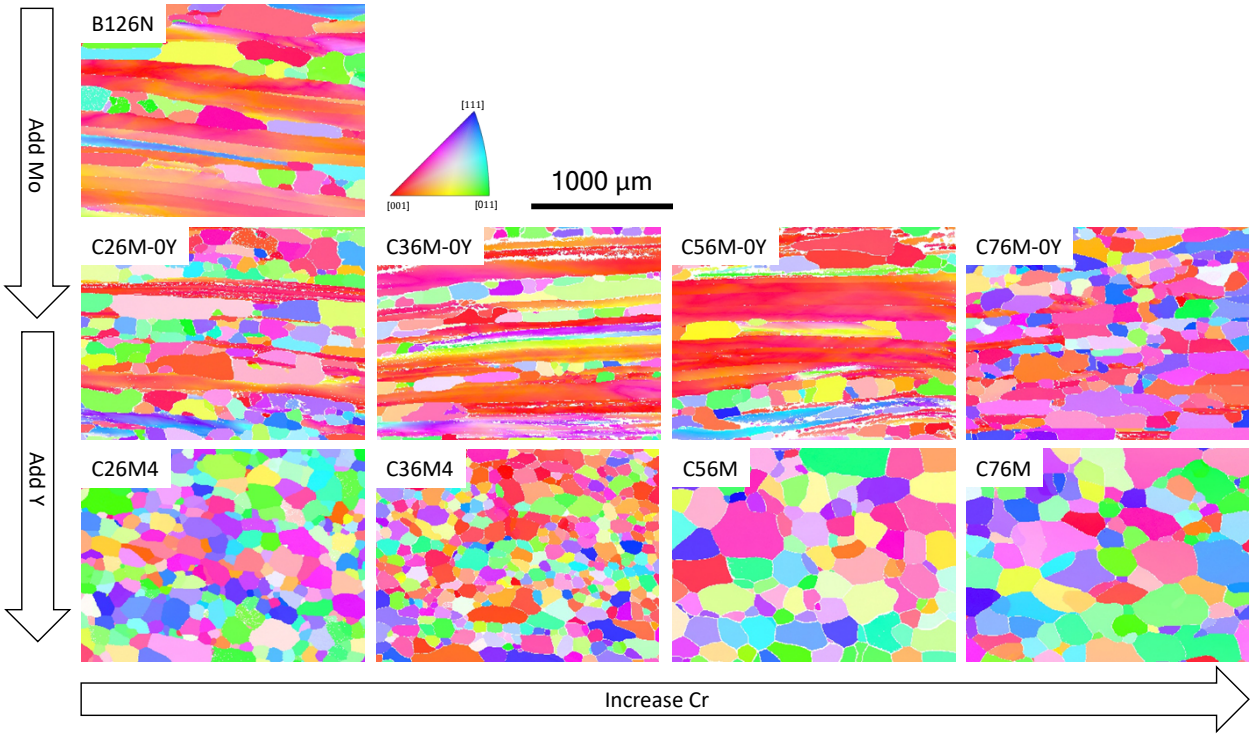

Figure 6. EBSD inverse pole figure (IPF) maps of various wrought FeCrAl alloys of interest for the current irradiation. In each figure, the IPF is taken with respect to the normal direction, and the prior rolling direction is horizontal.

The C26M ingot produced via HIP is shown in comparison to the wrought alloy in Figure 7. The HIP ingot was produced using a compressive stress of 150 MPa while holding at 1050°C for 3 h, which produced a 99.9% dense material. The grain size averages less than 20 µm, which is an order of magnitude lower than that of the ORNL-produced wrought FeCrAl alloys. The wrought FeCrAl alloy provided by GE for this irradiation also has an average grain size of 20 µm.

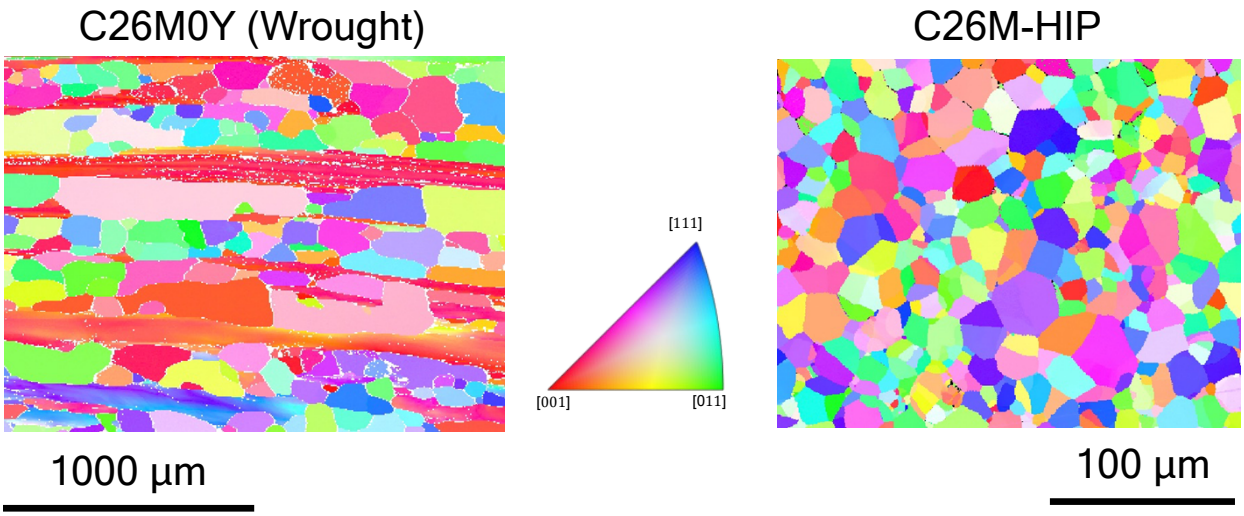

Figure 7. EBSD inverse pole figure maps of FeCrAl alloy Fe-12Cr-6Al-2Mo-0.2Si (nominal) produced in the wrought (C26M0Y) form as well as via HIP (C26M-HIP). Both alloys do not contain the trace amounts of yttrium normally expected in alloy C26M.

The EBSD IPF maps for the three wrought AFAs are shown in Figure 8. The grain structures of all three alloys were similar and did not show increased grain refinement as the niobium content increased from 0.6% (AA06) to 1.5% (AA09). Each of these materials showed similar precipitate distributions, an example of which is provided in Figure 9 for the AA06 alloy. Two types of precipitates were identified in each alloy, which appeared to be aligned along the prior rolling direction but distributed both along grain boundaries and within grain interiors. One distribution of precipitates was enriched primarily in nickel and aluminum, which is consistent with thermodynamic predictions of B2 phase within the alloys. The second distribution of precipitates was enriched in both niobium and molybdenum, and these are expected to be MX-type carbides. Future work will continue characterization of these new ATF cladding candidate alloys.

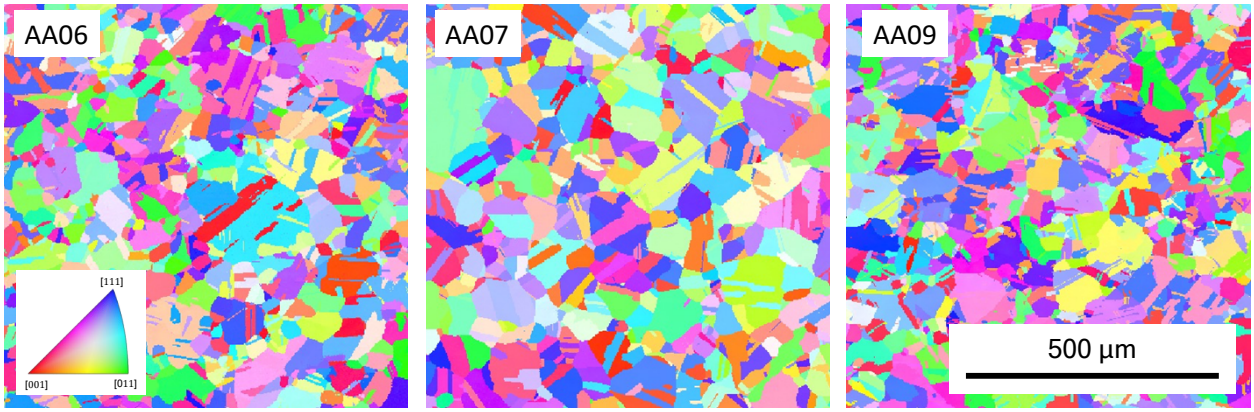

Figure 8. EBSD IPF maps of wrought AFAs (AA06, AA07, and AA09).

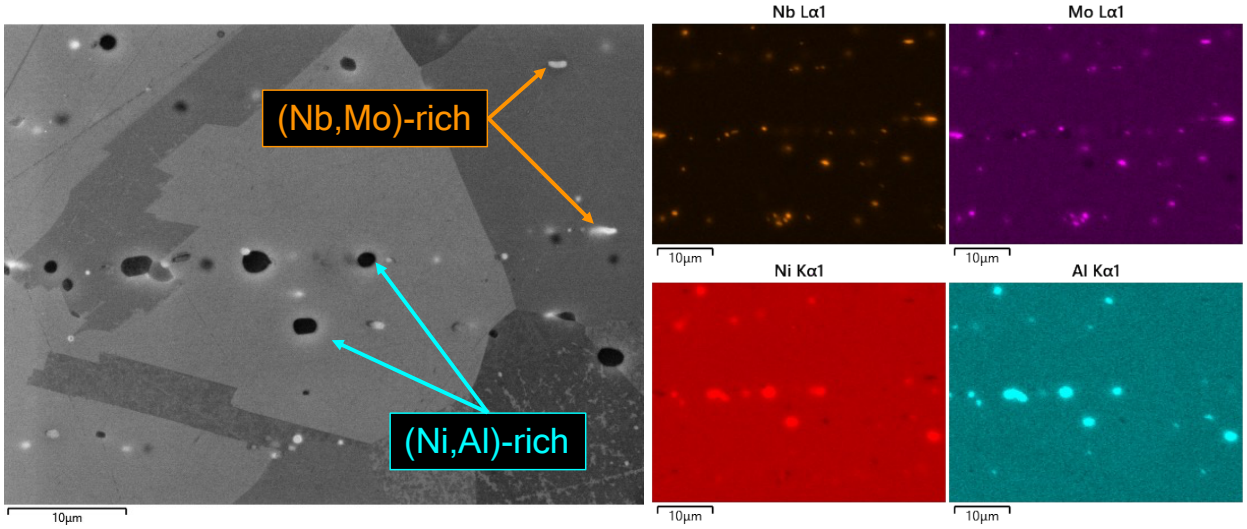

Figure 9. SEM+EDS elemental intensity maps for AA06, showing two different types of precipitates.

3.1.2 Mechanical properties

Mechanical properties were collected to provide baseline performance data before irradiation. Tensile tests were conducted at room temperature (RT), and additional specimens are scheduled to be tested at the target irradiation temperature. Fracture toughness tests were conducted at RT, again with eventual intent to collect data at the target irradiation temperature. Tensile tests were performed in air using a strain rate of 10^{-3} s^{-1}, whereas fracture testing was performed in a three-point bend configuration with a span of approximately 13 mm and at a displacement rate of 5 µm/s. For fracture toughness testing, each MBS-1 specimen was fatigue pre-cracked before being tested or assembled in an irradiation capsule. The pre-cracking and fracture toughness testing was performed on one of the two electromagnetic tensile frames (TestResources 810LE5 and 800LE3) each equipped with a cradle grip designed specifically for the MBS-1 specimen (see Figure 10). The static and fatigue load capacities of the larger (810LE5) and smaller (800LE3) frames are, respectively, ±24 kN and ±3.2 kN. Both are rated at 15 Hz for cyclic fatigue testing, and the larger frame is equipped with a 900°C-rated clamshell-type furnace.

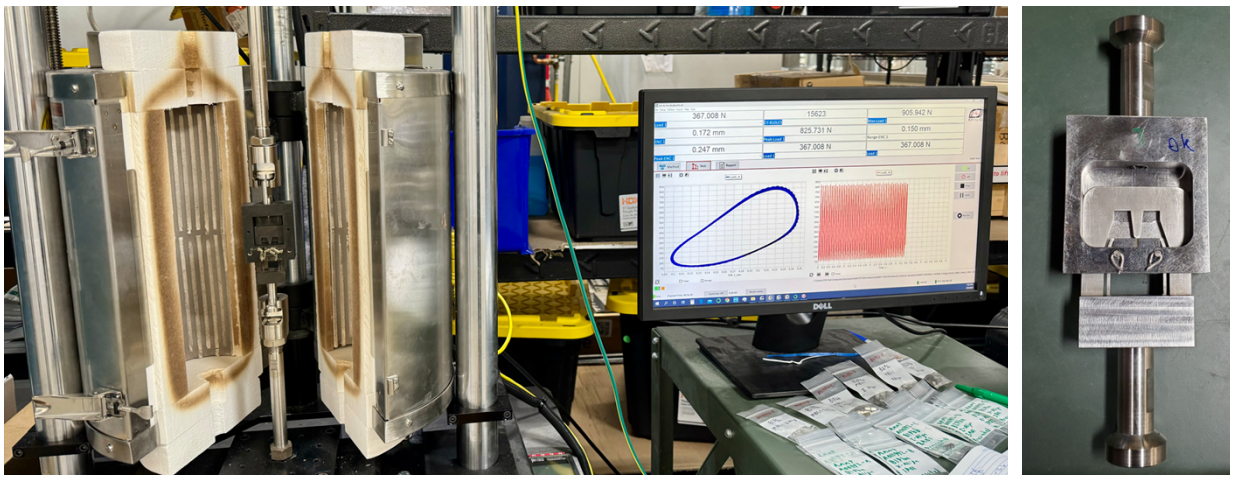

(a) (b)

Figure 10. Electromagnetic testing system TestResources 810E5-30: (a) overall view, and (b) detail of the cradle grip.

At this writing, tensile properties have been collected on all wrought FeCrAl and wrought AFA alloys at temperatures up to 800°C; the fracture characterization of these materials is ongoing. For the purposes of this report, however, a general snapshot of RT performance is provided for selected specimens to highlight the various hypotheses to be investigated during PIE. For example, Figure 11(a) highlights key differences in wrought FeCrAl alloys with and without molybdenum and yttrium addition. For the yttrium-free alloys, B126N and C26M0Y, total elongation exceeded 30%, with a well-defined necking behavior. However, the yttrium-containing alloy fractured prematurely in the strain hardening regime, which may be due to crack propagation assisted via embrittling intermetallic phases on the C26M grain boundaries. Post-irradiation tensile tests for these three alloys will indicate whether these trends continue, or whether all three alloys lose all ductility following irradiation. As a function of chromium content, however, no clear monotonic trends were observed with respect to strength or ductility in the unirradiated state (Figure 11(b)). Any compositional effects were overshadowed by the effects of grain structure. However, it is expected that following irradiation, the deformation mechanism will be dominated by the loop and chromium-rich precipitate structures, so post-irradiation strength and ductility may be different between these three alloys.

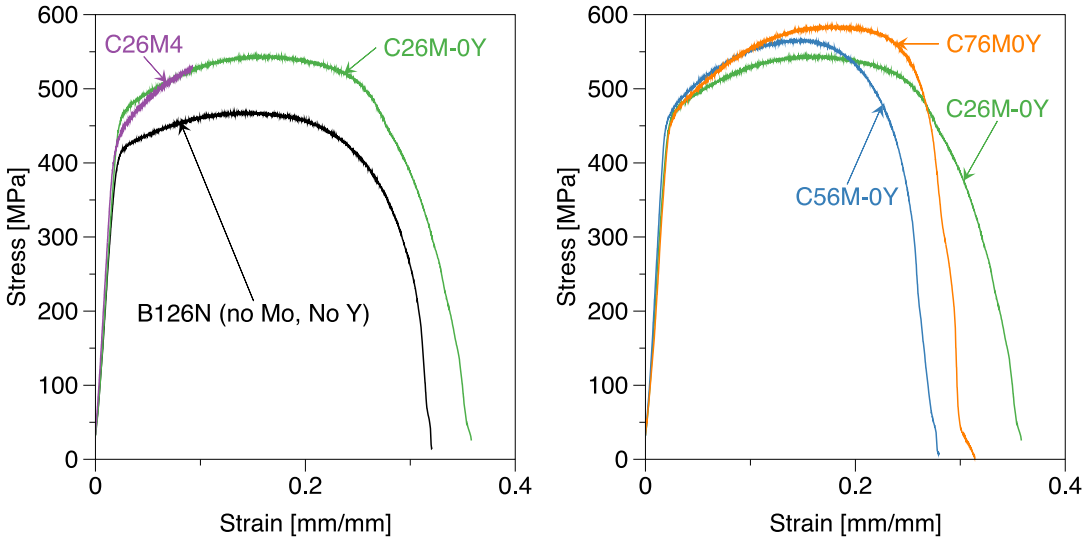

(a) (b)

Figure 11. RT engineering stress/strain curves for (a) three Fe-12Cr-6Al alloys with varied minor alloying concentrations and (b) as a function of increasing chromium content.

With respect to the various AFAs being scoped in this initial irradiation campaign, preliminary tensile and fracture toughness data are provided in Figure 12. AA06 has the lowest niobium content of the three alloys (0.6 wt.%), whereas AA07 and AA09 have 1% and 2.5% by weight, respectively. As niobium content increases, Figure 12 shows the resultant increase in both yield strength and ultimate tensile strength due to the increased precipitation. However, this increase in strength resulted in the concurrent decrease in fracture toughness (using $K_{0.2\ mm}$ values as calculated using ASTM E1820 and ASTM E399 standards) by a factor of 2. Since some loss of fracture toughness is also expected for the AFAs following lower temperature neutron irradiation, it is unclear whether the fracture toughness will remain superior to FeCrAl alloys due to the complex precipitation state in the AFA materials. This same concern exists for the high-strength LBPF AFA05 alloy, which shows double the strength of the wrought and recrystallized AFA materials.

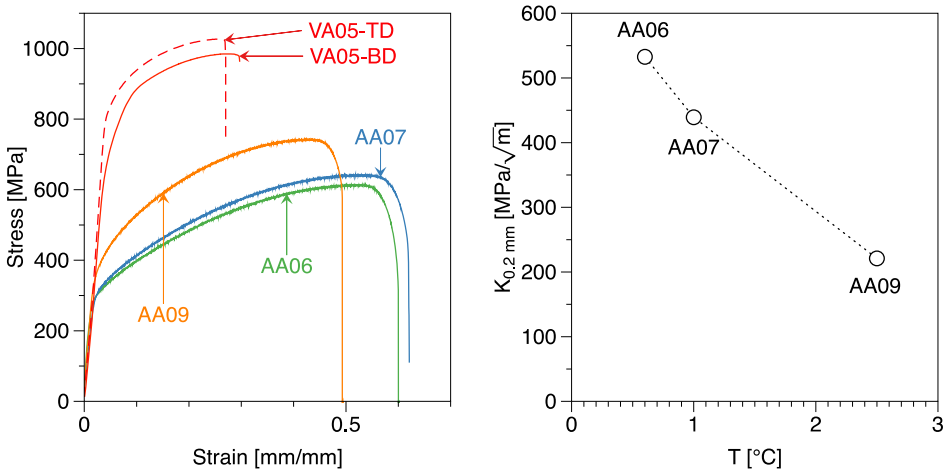

(a) (b)

Figure 12. RT (a) engineering stress/strain curves and (b) fracture toughness values for the three wrought AFAs analyzed in this work. In (a), the tensile properties of the LPBF AFA (AFA05) in both the build direction (BD) and transverse direction (TD) are also shown to highlight its higher strength in comparison to conventional wrought alloys, hence its inclusion in this irradiation campaign.

3.2 Test Matrix

The irradiation test matrix corresponding to this work includes two GENTEN capsules and four MINBEN capsules. The capsules target an irradiation damage of either 2 or 8 dpa, corresponding to 1 and 4 HFIR cycles, respectively. The details of the test matrix are shown in Table 4.

Table 4. Irradiation test matrix.

Capsule ID	Capsule design	Specimens	Temperature	dose (dpa)	No. of HFIR cycles	Alloy	Number of specimens
AFT-1	GENTEN	SS-J2	315°C	2	1	AA06	4
						AA07	4
						AA09	4
						B126N	4
						C26M0Y	4
						C56M0Y	4
						C76M0Y	4
						C26M4	2
						C26M-HIP	2
						AFA05-LPBF-BD	2
						AFA05-LPBF-TD	2
AFT-2				8	4	AA06	4
						AA07	4
						AA09	4
						B126N	4
						C26M0Y	4
						C56M0Y	4
						C76M0Y	4
						C26M4	2
						C26M-HIP	2
						AFA05-LPBF-BD	2
						AFA05-LPBF-TD	2
AFF-1	MINBEN	MBS-1		2	1	AA06	2
						AA07	2
						AA09	2
AFF-2						C26M4	2
						C26M-W	2
						C26M0Y	2
AFF-3				8	4	AA06	2
						AA07	2
						AA09	2
AFF-4						C26M4	2
						C26M-W	2
						C26M0Y	2

4. CAPSULE ASSEMBLY

To date, two MINBEN capsules (AFF-3 and AFF-4 – see Table 4) have been fully assembled and are ready for insertion in HFIR. These capsules were built using aluminum holders with a 9.27 mm OD, 100% helium fill gas, and are intended for insertion in HFIR cycle 506 (starting in April 2024) in position TRRH-4 (C1-4 and A3-4, respectively). This combination of holder material/holder OD/gas fill/TRRH position allows the target temperature specified in the test matrix to be met (see Table 4). These capsules are expected to complete irradiation after HFIR cycle 509 (September 2024). Figure 13 shows the capsule parts layout for capsule AFF-3 and Figure 14 shows the two capsules fully assembled, welded, and ready for insertion.

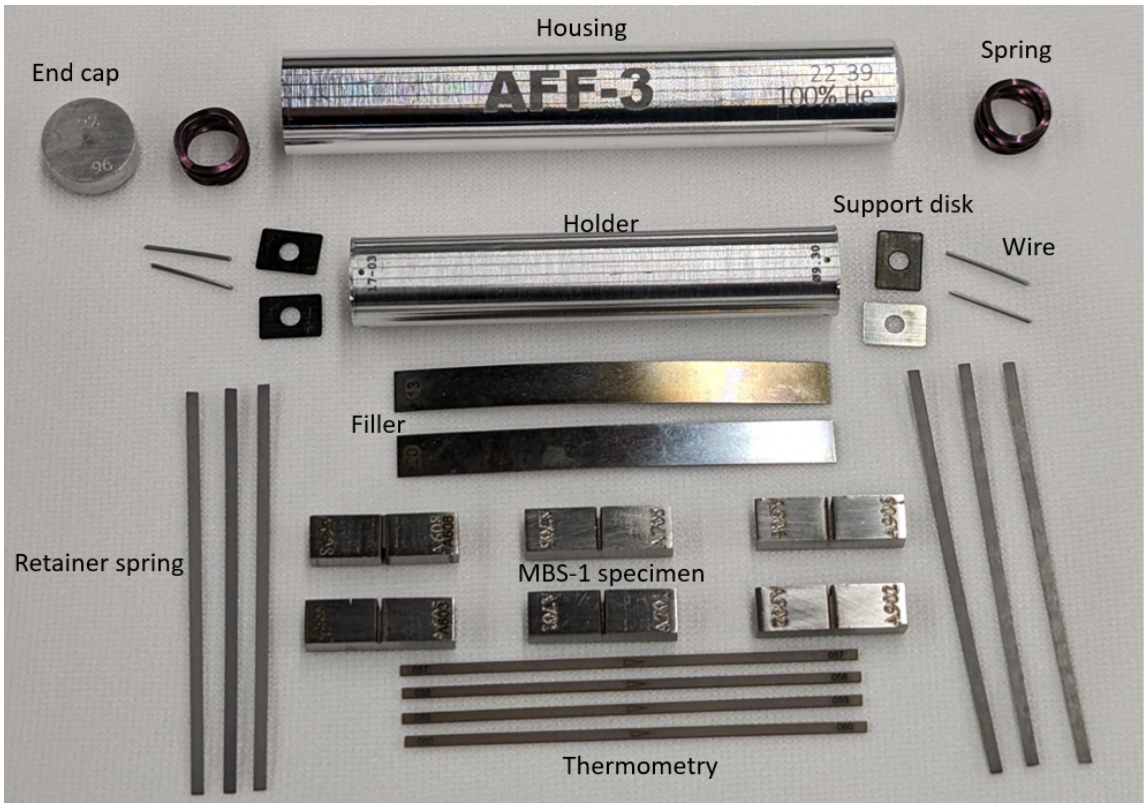

Figure 13. Example of MINBEN capsule parts layout.

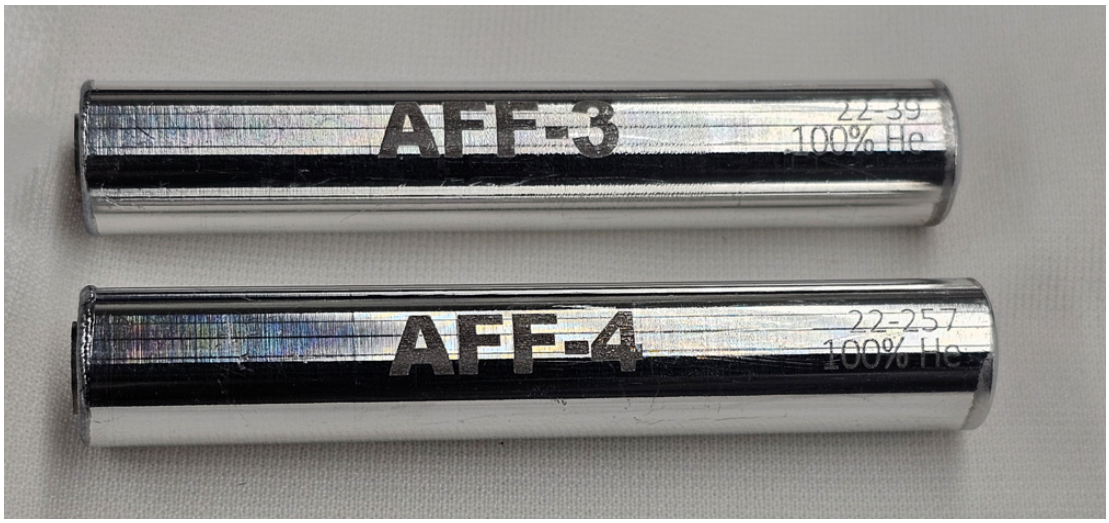

Figure 14. Capsules AFF-3 and AFF-4 fully assembled.

The assembly of the four other capsules is under preparation. The design parameters used for these irradiation capsules are as follows:

- AFT capsules: 9.23 mm OD Al holder, position TRRH 3/5, 100% He fill gas
- AFF capsules: 9.26 mm OD Al holder, position TRRH 3/5, 100% He fill gas

These capsules are intended for insertion in HFIR cycle 507 (June 2024) and will complete irradiation at the end of cycle 507 (July 2024) and cycle 510 (November 2024) for the lower-dose and higher-dose capsules, respectively. Table 5 summarizes the timeline for irradiation of each capsule of the test matrix (see Table 4).

Table 5. Anticipated start and end of irradiation.

Capsule ID	Target start of irradiation	Expected irradiation completion
AFT-1	Cycle 507 (June 2024)	Cycle 507 (July 2024)
AFT-2	Cycle 507 (June 2024)	Cycle 510 (November 2024)
AFF-1	Cycle 507 (June 2024)	Cycle 507 (July 2024)
AFF-2	Cycle 507 (June 2024)	Cycle 507 (July 2024)
AFF-3	Cycle 506 (April 2024)	Cycle 509 (September 2024)
AFF-4	Cycle 506 (April 2024)	Cycle 509 (September 2024)

5. PIE PLAN

The PIE plan includes tensile testing at RT and irradiation temperature, fracture toughness testing at irradiation temperature, and microstructure characterization using transmission electron microscopy (TEM) liftouts with scanning TEM (STEM) and EDS characterization for each alloy part of the test matrix. Fracture toughness testing at RT could also be performed if needed. Table 6 summarizes the PIE plan for this irradiation campaign.

Table 6. Summary of the PIE plan.

Alloy	Irradiation damage	Specimen type	Testing/ Analysis	Test condition	No. of specimens to be tested
Each alloy	2 dpa	SS-J2	Tensile	RT	2
				Irradiation temp.	2
		MBS-1	Fracture toughness	RT	1
				Irradiation temp.	1
		Sample of any specimen	Microstructure	TEM/STEM/EDS	1
	8 dpa	SS-J2	Tensile	RT	2
				Irradiation temp.	2
		MBS-1	Fracture toughness	RT	1
				Irradiation temp.	1
		Sample of any specimen	Microstructure	TEM/STEM/EDS	1

6. CONCLUSIONS

The AFC irradiation testing of FeCrAl/AFA tensile and bend bar specimens at ORNL aims to (1) study the effects of composition (molybdenum and yttrium) and processing methodology (HIP vs. wrought C26M) on neutron irradiation hardening and embrittlement of conventional FeCrAl alloys, and (2) quantify the deterioration of AFA alloys' fracture toughness as a function of niobium content and compare their irradiated properties with those of conventional FeCrAl alloys.

A test matrix including tensile and bend bar specimens from various conventional FeCrAl/AFA alloys has been developed. The irradiation conditions of interest are a target temperature of 315°C and irradiation damage levels of 2 and 8 dpa. Pre-characterization work on each of these alloys included SEM and mechanical testing. The first 2 irradiation capsules have been fully assembled and are ready for insertion in HFIR cycle 506 (April 2024). The assembly of the remaining irradiation capsules is under preparation. These capsules are planned for insertion in HFIR cycle 507 (June 2024).

The PIE plan includes tensile testing at RT and irradiation temperature, fracture toughness testing at irradiation temperature, and TEM liftouts with STEM/EDS characterization.

7. REFERENCES

[1] M. Snead, L. Snead, K.A. Terrani, K.G. Field, A. Worrall, K.R. Robb, Y. Yamamoto, J. Powers, S. Dryepondt, B.A. Pint, "Technology Implementation Plan ATF FeCrAl Cladding for LWR Application," ORNL/TM-2014/353, Oak Ridge National Laboratory, Oak Ridge, TN (2014).

[2] K.S. Mao, C.P. Massey, Y. Yamamoto, K.A. Unocic, M.N. Gussev, D. Zhang, S.A. Briggs, O. Karakoc, A.T. Nelson, K.G. Field, P.D. Edmondson, *Improved Irradiation Resistance of Accident-Tolerant High-Strength FeCrAl Alloys with Heterogeneous Structures*, Acta Materialia (2022).

[3] X. Chen, K.G. Field, R. Howard, C.P. Massey, A.T. Nelson, "Post-Irradiation Fracture Toughness Characterization of Generation II FeCrAl Alloys," ASME 2022 Pressure Vessels & Piping Conference (2022).

[4] K.S. Mao, C.P. Massey, M.N. Gussev, Y. Yamamoto, A.T. Nelson, K.G. Field, P.D. Edmondson, *Irradiation-induced amorphization of Fe-Y-based second phase particles in accident-tolerant FeCrAl alloys*, Materialia 15 (2021).

[5] K.G. Field, K.C. Littrell, S.A. Briggs, *Precipitation of α' in neutron irradiated commercial FeCrAl alloys*, Scripta Materialia **142** (2018) 41–45.

[6] S.A. Briggs, P.D. Edmondson, K.C. Littrell, Y. Yamamoto, R.H. Howard, C.R. Daily, K.A. Terrani, K. Sridharan, K.G. Field, *A combined APT and SANS investigation of α ' phase precipitation in neutron-irradiated model FeCrAl alloys*, Acta Materialia **129** (2017) 217–228.

[7] P.D. Edmondson, S.A. Briggs, Y. Yamamoto, R.H. Howard, K. Sridharan, K.A. Terrani, K.G. Field, *Irradiation-enhanced α ' precipitation in model FeCrAl alloys*, Scripta Materialia **116** (2016) 112–116.

[8] K.G. Field, X. Hu, K.C. Littrell, Y. Yamamoto, L.L. Snead, *Radiation tolerance of neutron-irradiated model Fe–Cr–Al alloys*, Journal of Nuclear Materials **465** (2015) 746–755.

[9] M.P. Brady, J. Magee, Y. Yamamoto, D. Helmick, L. Wang, *Co-optimization of wrought alumina-forming austenitic stainless steel composition ranges for high-temperature creep and oxidation/corrosion resistance*, Materials Science and Engineering: A **590** (2014) 101–115.

[10] B.A. Pint, Y.-F. Su, M.P. Brady, Y. Yamamoto, J. Jun, M.R. Ickes, *Compatibility of Alumina-Forming Austenitic Steels in Static and Flowing Pb*, JOM **73**, issue 12 (2021) 4016–4022.

[11] "High Flux Isotope Reactor (HFIR) User Guide – A guide to in-vessel irradiations and experiments", Revision 2.0, Oak Ridge National Laboratory (2015).

[12] P.A. Champlin, J. Burns, C.M. Petrie, X. Hu, K.D. Linton, R. Howard, K.A. Terrani, "Capsule and Specimen Geometries for HFIR Irradiation Testing Supporting the Transformational Challenge Reactor," ORNL/TM-2019/1310, Oak Ridge National Laboratory, Oak Ridge, TN (2019).

[13] P.A. Champlin, C.P. Massey, A.G. Le Coq, S.A. Taller, T.S. Byun, K.D. Linton, "AMMT FY23 HFIR Irradiation Test Matrix – Supported by the Design of a Miniature Bend Bar Irradiation Vehicle," ORNL/TM-2023/3037, Oak Ridge National Laboratory, Oak Ridge, TN (2023).

[14] K.G. Field, J.L. McDuffee, J.W. Geringer, C.M. Petrie, Y. Katoh, *Evaluation of the continuous dilatometer method of silicon carbide thermometry for passive irradiation temperature determination*, Nuclear Inst. And Methods in Physics Research B, **445** (2019), pp 46–56.

[15] K.G. Field, X. Hu, K.C. Littrell, Y. Yamamoto, L.L. Snead, *Radiation tolerance of neutron-irradiated model Fe–Cr–Al alloys*, Journal of Nuclear Materials, **465** (2015), pp 746–755.

[16] C.P. Massey, D. Zhang, S.A. Briggs, P.D. Edmondson, Y. Yamamoto, M.N. Gussev, K.G. Field, *Deconvoluting the Effect of Chromium and Aluminum on the Radiation Response of Wrought FeCrAl Alloys After Low-Dose Neutron Irradiation*, Journal of Nuclear Materials, **549** (2021).